Bone forming ability of recombinant human collagen peptide granules applied with β-tricalcium phosphate fine particles

Tomokazu Furihata[1], Hirofumi Miyaji[1], Erika Nishida[1], Akihito Kato[1], Saori Miyata[1], Kanako Shitomi[1], Kayoko Mayumi[1], Yukimi Kanemoto[1], Tsutomu Sugaya[1], Tsukasa Akasaka[2]

Institutions

[1]Department of Periodontology and Endodontology, [2]Department of Biomedical Materials and Engineering, Faculty of Dental Medicine, Hokkaido University. N13, W 7, Kita-ku, Sapporo 060-8586, Japan

Corresponding author

Hirofumi MIYAJI

Department of Periodontology and Endodontology, Faculty of Dental Medicine, Hokkaido University. N13, W 7, Kita-ku, Sapporo 060-8586, Japan

Running Head

Bone forming granules with recombinant collagen peptide and β-TCP

Key words

Bone filling material, integrin β1, osteogenic differentiation, rat skull, recombinant peptide based on human collagen type I

Abstract

Recombinant human collagen peptide, developed based on human collagen type I, contains an arginyl-glycyl-aspartic acid (RGD)-rich motif to enhance cell behavior and is anticipated as a xeno-free polymer material for use in tissue engineering. We fabricated granules containing recombinant human collagen peptide (RCP) applied with beta-tricalcium phosphate fine particles (RCP/β-TCP) as bone filling scaffold material and assessed the bone forming ability of RCP/β-TCP.

Recombinant peptide was thermal crosslinked and freeze-dried to prepare RCP. An aqueous dispersion of β-TCP fine particles was added to RCP to obtain RCP/β-TCP. Subsequently, RCP/β-TCP were characterized using scanning electron microscopy (SEM), energy dispersive X-ray spectrometry (EDX), and cell culture assessments. Furthermore, RCP/β-TCP were implanted into rat cranial bone defects for radiographic and histological evaluations.

In SEM and EDX analyses of RCP/β-TCP, β-TCP particles dose-dependently covered the surface of RCP. Cell culture tests showed that RCP/β-TCP remarkably promoted proliferation and mRNA expression of various genes, such as integrin β1 and osteogenic markers, of osteoblastic MC3T3-E1 cells. Histomorphometric assessment at 4 weeks showed that RCP/β-TCP significantly promoted new skull bone formation compared to RCP ($P<0.05$) and control (no application) ($P<0.01$). Accordingly, these findings suggest RCP/β-TCP possess bone forming capability and would be beneficial for bone tissue engineering therapy.

1 Introduction

Improvement of bone tissue engineering therapy is required for the treatment of bone loss caused by infectious disease, trauma, and cancer. Three elements of tissue engineering are proposed (OKeefe, & Mao, 2011) ; cells (Diederichs et al., 2010; Fawzy El-Sayed et al., 2015; Perez et al., 2018), signaling molecules (Peticone et al., 2017; Kim, Lee, & Kim, 2018; Yin et al., 2018), and natural and artificial scaffolds (Xing et al., 2013; Carrel et al., 2016; Nathanael et al., 2017) are essential for bone conductive strategies. Scaffolds play a major role in stimulating cell proliferation and differentiation and providing growth and nutrition factors in bone defects (Bose, Roy, & Bandyopadhyay, 2012). The polymer matrix is widely known as a good bioabsorbable scaffold material (Sheikh et al., 2016; Hamlet, Vaquette, Shah, Hutmacher, & Ivanovski, 2017). Especially, collagen type I has great cellular affinity and biodegradability as scaffold material (Kuttappan, Mathew, & Nair, 2016). However, the bone forming ability of collagen is low compared with bioceramics (Ogawa et al., 2016; Murakami et al., 2017). In addition, collagen type I containing clinical conventional scaffold is obtained from xenogeneic tissues such as bovine and porcine tissues, which may increase the risk of unknown pathogens (Ogawa et al., 2016; Murakami et al., 2017; Nathanael et al., 2017; Cuervo-Lozano et al., 2018). Hence, new collagen scaffold material and application are needed to overcome the disadvantages of collagen substrate.

Recently, gene recombination technology has been introduced to improve the problem of xenogeneic materials (Thomason, Sawitzke, Li, Costantino, & Court, 2014; Zhu et al., 2020). Pawelec et al. described the biocompatibility of recombinant human collagen peptide scaffold (Pawelec et al., 2017). The peptide is based on human

collagen type I and recombinantly enriched with arginyl-glycyl-aspartic acid (RGD) groups to contribute to cell adhesion and osteoblastic differentiation (Parvizi et al., 2016; Pawelec et al., 2017). In addition, some reports showed the characteristics of recombinant peptide as the scaffold of bone marrow stromal cell and adipose-derived stem cells (Mashiko et al., 2018; Miyamoto et al., 2018). Therefore, it is likely that recombinant peptide can innovate bone tissue engineering therapy.

Bio-safe and absorbable bioceramics, such as beta-tricalcium phosphate (β-TCP), have been clinically applied to bone graft materials (Zijderveld, Zerbo, van den Bergh, Schulten, & ten Bruggenkate, 2005; Kakar et al., 2017). β-TCP grafts possess the properties of bioresorption in the body, unlike hydroxyapatite grafts, and continuous Ca and P ion supplying ability to stimulate bone formation (Oh, Ko, Jaiswal, & Whang, 2016). Reportedly, collagen scaffold coated with β-TCP fine particles showed increased bioactive effects such as cell proliferation, protein adsorption, and bone tissue regeneration (Ibara et al., 2013; Ogawa et al., 2016; Murakami et al., 2017). Murakami et al. revealed that collagen scaffold containing β-TCP fine particles stimulated not only bone formation but also bioresorption compared with collagen scaffold only (Murakami et al., 2017). Hence, application of β-TCP fine particles is suspected to upregulate the quality and quantity of newly engineered bone.

Accordingly, we hypothesized that recombinant peptide in combination with β-TCP fine particles exhibits bone forming and bioresorbing ability. We prepared granules containing recombinant human collagen peptide (RCP) applied with β-TCP fine particles (RCP/β-TCP) as the bone filling scaffold material and assessed osteoblastic cellular responses and bone forming ability.

2 Materials and Methods

2.1 Preparation of RCP/β-TCP

An aqueous solution of recombinant human collagen peptide (7.5%, cellnest^{TM}, FUJIFILM Wako Pure Chemical Corp., Osaka, Japan) was freeze-dried and pulverized into approximately 1-mm granules by a granulator (Quadro Comil U5, Quadro Engineering Corp., Waterloo, Canada). Subsequently, thermal crosslinking at 142°C for 5 h was carried out using a vacuum drying oven (DP-43, Yamato Scientific Co., Ltd., Tokyo, Japan) to obtain RCP. The size of RCP was measured as mass-median-diameter (D_{50}) using a static image analysis system (Morphologi G3, Malvern Panalytical Ltd., Malvern, UK). β-TCP (β-TCP-100 milled product, Taihei Chemical Industrial Co., Ltd., Osaka, Japan) was pulverized into submicron size by the Nanovater (NVL-AS200-D10, Yoshida Kikai Co., Ltd., Nagoya, Japan) and dispersed into water. The particle size of β-TCP was measured as D_{50} using a particle size distribution measuring apparatus (SALD-2100, Shimadzu Corp., Kyoto, Japan). Subsequently, 500 μL of β-TCP dispersion (concentrations: 0, 0.01, 0.1, and 1 wt%) were added into 100 mg freeze-dried RCP to swell (Fig. 1A).

2.2 Morphological assessments

Each sample was analyzed using a scanning electron microscope (SEM, S-4000, Hitachi, Ltd., Tokyo, Japan) at an accelerating voltage of 10 kV after coating with a thin layer of Pt-Pd. In addition, the sample surface was characterized using energy dispersive X-ray spectrometry (EDX, JSM-6500F, JEOL Ltd., Tokyo, Japan).

2.3 Assessments of cytocompatibility

RCP or RCP/β-TCP (100 mg) were placed at the bottom of wells in a 48-well plate. Mouse osteoblastic MC3T3-E1 cells (RIKEN BioResource Center, Tsukuba, Japan) were seeded onto the samples (1×10^4 cells/0.5 mL/well) and incubated in a humidified atmosphere containing 5% CO_2 at 37°C using culture medium (MEM alpha, GlutaMAX-I, Thermo Fisher Scientific, Waltham, MA, USA) supplemented with 10% fetal bovine serum (Qualified FBS, Thermo Fisher Scientific) and 1% antibiotics (penicillin-streptomycin, Thermo Fisher Scientific).

Assessments of cell proliferation and cytotoxicity at 3 and 7 days of culture were carried out using water-soluble tetrazolium salt (WST)-8 (Cell Counting Kit-8, Dojindo Laboratories, Mashiki, Japan) and lactate dehydrogenase (LDH, Cytotoxicity LDH Assay Kit-WST, Dojindo Laboratories) assays, respectively. The absorbance at 450 nm (WST-8) and 492 nm (LDH) was measured using a microplate reader (Multiskan™ FC, Thermo Fisher Scientific).

For the cell adhesion assay, cells were cultured for 24 h, washed with phosphate-buffered saline (PBS, FUJIFILM Wako Pure Chemical Corp.), and fixed with 3.5% formaldehyde. A staining solution was prepared by mixing 0.12 μg/mL phalloidin (Acti-stain 555 fluorescent phalloidin, Cytoskeleton Inc., Denver, CO, USA) dissolved in methanol, and 6.0 μg/mL 4’,6-diamidino-2-phenylindole solution (Dojindo Laboratories) in bovine serum albumin (7.5% w/v Albumin Dulbecco’s-PBS (−) Solution from bovine serum, FUJIFILM Wako Pure Chemical Corp.). Samples were immersed in this solution overnight at 4°C to stain cultured cells and then washed with PBS. The stained cells were observed using a fluorescence microscope (BioRevo BZ-9000, Keyence Corp., Osaka, Japan).

Some samples were stained using the LIVE/DEAD Viability/Cytotoxicity Kit for

mammalian cells (Thermo Fisher Scientific), following the manufacturer's instructions. Stained samples were also examined using a fluorescence microscope.

2.4 Real-time reverse transcription polymerase chain reaction (RT-PCR) assays

MC3T3-E1 cells were seeded (1×10^6 cells/0.5 mL/well) and grown on RCP or RCP/1% β-TCP (100 mg) in 48-well plates, using MEM supplemented with 10% FBS and 1% antibiotics. Cultures were incubated at 37°C with 5% CO_2. The medium was exchanged every 2 days. After 14 days, total RNA of cultured cells was extracted using TRIzol™ reagent (Invitrogen, Carlsbad, CA, USA) according to the manufacturer's instructions. Reverse transcription was conducted with 1 μg of RNA to obtain cDNA. The cDNA was amplified by ReverTra Ace-α FSK-101 (Toyobo Co., Ltd., Osaka, Japan). Real-time PCR (ABI Prism 7300 sequence detection system, Applied Biosystems, Carlsbad, CA, USA) was performed using primers (Applied Biosystems) for the following mouse genes: integrin β1 (*ITGB1*, Mm01253230_m1), runt-related transcription factor 2 (*RUNX2*, Mm00501584_m1), alkaline phosphatase (*ALP*, Mm00475834_m1), bone sialoprotein (*IBSP*, Mm00492555_m1), and glyceraldehyde-3-phosphate dehydrogenase (*GAPDH*, Mm99999915_g1). Data obtained for each sample were standardized against the expression of *GAPDH* and were calculated using the 2-ΔΔCt method (Schmittgen, & Zakrajsek, 2000; Pfaffl, 2001).

2.5 Animal procedure

Twenty-four 10-week-old male Wistar rats weighing approximately 190–210 g were used for this experiment. *In vivo* experiments in rats were carried out in accordance with the institutional animal use and care regulations of Hokkaido

University (Animal Research Committee of Hokkaido University, Approval number 16-29) and approved by the Animal Research Committee of Hokkaido University. Surgical procedures were performed under general anesthesia by intraperitoneal injection of medetomidine hydrochloride (0.15 mL/kg, Domitor, Nippon Zenyaku Kogyo Co., Ltd., Koriyama, Japan), midazolam (0.4 mL/kg, Dormicum®, Astellas Pharma Inc., Tokyo, Japan), butorphanol tartrate (0.5 mL/kg, Vetorphale, Meiji Seika Pharma Co., Ltd., Tokyo, Japan), and local injection of 2% lidocaine hydrochloride with 1:80,000 epinephrine (Xylocaine Cartridge for Dental Use, Dentsply Sirona K.K., Tokyo, Japan).

After elevation of the skin-periosteal flap, bone defects with a 4.5-mm diameter were created on the cranial bone with a trephine bar (Meis Trephine bar, Hager & Meisinger GmbH, Neuss, Germany) operating at 1500 rpm/min or less. Subsequently, defects were filled with RCP or RCP/1% β-TCP (4 mg/defect, Fig. 1B). No implantation was performed as the negative control. After that, skin was sutured (BioFit-D 4-0; Washiesu Medical Corp., Tokyo, Japan) and applied with tetracycline hydrochloride (Achromycin ointment, Pola Pharma Inc., Tokyo, Japan) to prevent postoperative infection.

2.6 X-ray micro-computed tomography assessments

At 2 and 4 weeks postsurgery, rats were euthanized using an overdose of sodium pentobarbital (2.0 mL/kg, Somnopentyl, Kyoritsu Seiyaku Corp., Tokyo, Japan). Samples were fixed in 10% buffered formalin and assessed by X-ray micro-computed tomography scanner (Latheta LCT-200, Hitachi, Ltd., scanning protocol: 50 kV voltage, 500 μA current, no filter, 60 μm pixel size and 0.1° rotation angle). From the captured

micro-CT images, percent bone volume (BV/TV) was measured using ImageJ software package (ImageJ 1.41; National Institutes of Health, Bethesda, MD, USA).

2.7 Histological observations

Samples were decalcified in 10% ethylenediaminetetraacetic (EDTA) acid, embedded in paraffin, and sliced for hematoxylin-eosin (HE) and Masson's trichrome (MT) staining. In addition, immunohistochemical analysis was conducted using 2-week postsurgery samples. After the heat-induced epitope retrieval step (95°C) in citrate buffer (pH 6) or tris-EDTA buffer (pH 9), sections were incubated overnight with the following primary antibodies: mouse anti-CD68 (1:100 dilution; Bio-Rad Laboratories Inc., Hercules, CA, USA) or rabbit anti-osteocalcin antibody (1:200 dilution; Proteintech Group Inc., Chicago, IL, USA). Antigen–antibody reaction sites were detected by incubation with anti-mouse or rabbit IgG labeled with Cy3 fluorescent dye (Jackson ImmunoResearch Inc., West Grove, PA, USA). Nuclear staining was performed using DAPI (Dojindo Laboratories). Sections were observed under a fluorescence microscope. For histomorphometric analyses, images of 2- and 4-week samples stained with HE were taken using light microscopy. The area of newly formed bone was measured using the ImageJ software package.

2.8 Statistical analysis

Means and standard deviations of each parameter were calculated for each group. Differences between the groups were analyzed using the Kruskal-Wallis test with multiple comparisons. *P*-values < 0.05 were considered statistically significant. All

statistical procedures were performed using SPSS 11.0 (IBM Corp., Armonk, NY, USA).

3 Results

3.1 Characterization of RCP/β-TCP

D_{50} of RCP (no application of β-TCP) and β-TCP particles were determined as 1170.8 and 0.7 μm, respectively. SEM showed that RCP had a rugged surface and pore-like structures (Fig. 1C). RCP/β-TCP showed that β-TCP fine particles dose-dependently covered the surface of RCP (Fig. 1D–F). In coating with 1% β-TCP dispersion, the layer of aggregated β-TCP particles mostly covered the surface of RCP (Fig. 1F). EDX mapping analysis of the surface of RCP/β-TCP confirmed the presence of P and Ca (Fig. 2). The intensity of P and Ca increased with increasing β-TCP concentration in a dose-dependent manner.

3.2 Cytocompatibility of RCP/β-TCP

The results of WST-8 and LDH assays are presented in Fig. 3A and B. All samples showed increased WST-8 activity from 3 to 7 days. RCP/1% β-TCP exhibited 1.6-fold greater WST-8 activity than RCP at 7 days ($P<0.01$) (Fig. 3A). In addition, LDH activity of RCP/β-TCP was equivalent or low compared with RCP through all experimental periods, and RCP/0.01% and 0.1% β-TCP at 3 days and RCP/0.01% and 1% β-TCP at 7 days were significantly lower than that of RCP, respectively ($P<0.05$) (Fig. 3B).

Cells cultured with RCP and RCP/β-TCP expressed actin as evidence of cell attachment and spreading, regardless of the concentration of β-TCP fine particles. In

addition, the LIVE/DEAD BacLight assay showed that all samples consistently exhibited live cells (Fig. 3C).

3.3 RT-PCR assays

Measurements of amplified cDNA by real-time RT-PCR showed that RCP and RCP/1% β-TCP had significantly higher expression of collagen-binding protein, integrin β1, and osseous markers *Runx2*, *Alp*, and *IBSP* than control (no application of RCP or RCP/β-TCP) ($P<0.05$). No significant difference was found between RCP and RCP/β-TCP (Fig. 4).

3.4 Assessment of bone formation by micro-CT image

Micro-CT images taken at 2 and 4 weeks postsurgery are shown in Fig. 5A. In the control group (no application of RCP or RCP/β-TCP), radiopacity of the cranial bone created by trephine bur was rarely increased at 2 weeks. In contrast, implantation of RCP or RCP/1% β-TCP increased radiopacity. In addition, radiopacity was rarely increased at 4 weeks in control specimens, similar to 2-week postsurgery samples. By contrast, images taken of RCP and RCP/β-TCP groups showed increased radiopacity that frequently appeared at the center of the bone defect. BV/TV of control, RCP, and RCP/β-TCP was 12.0, 8.6, and 50.1 at 2 weeks and 12.4, 52.3, and 70.4 at 4 weeks postsurgery, respectively. At 2 weeks postsurgery, BV/TV of RCP/β-TCP was significantly higher than those of control and RCP ($P<0.05$). The increase in BV/TV of RCP, as well as RCP/β-TCP, had progressed at 4 weeks and significant differences were found compared to control ($P<0.01$) (Fig. 5B).

3.5 Histological evaluation

Fig. 6 shows histological evaluation of RCP/1%β-TCP specimens obtained at 2 weeks postsurgery. In HE-stained sections, new bone formation was found around and in the inner region of implanted RCP/β-TCP. Pore and mesh structures of RCP were absent and bone tissue directly deposited into the pores. Bone tissue was defined as collagen-rich bone tissue by MT staining. Severe inflammatory response and remnant β-TCP particles were not found around RCP/β-TCP. CD68 immunostaining indicated that CD68-positive macrophages were frequently observed around RCP/β-TCP. However, areas of new bone formation had few CD68-positive cells. Osteocalcin immunostaining showed that osteocalcin-positive osteoblastic cells were aligned to the surface of newly formed bone tissue. Osteoblastic cells were also detected on the surface of RCP/β-TCP in areas without bone formation.

Four-week postsurgery specimens were observed to compare the areas of newly formed bone (Fig. 7). In the control group, bone defects were occupied with sparse fibrous connective tissue and new bone formation was slight and continuous with preexisting bone. In contrast, RCP and RCP/β-TCP applied groups showed remarkable bone formation. Especially, RCP/β-TCP showed thick and a large amount of new bone, which fully occupied the bone defect. Bone tissue was partly deposited to fill the meshwork structure of RCP, similar to 2-week postsurgery samples. In addition, blood vessels were frequently observed in newly formed bone tissue. TCP fine particles or aggregation were not found in the implantation area. The bone formation area ($\times 10^2$, pixel) of control, RCP, and RCP/β-TCP groups at postsurgery measured 3.4, 3.2, and 17.2 at 2 weeks and 2.3, 14.7, and 33.4 at 4 weeks, respectively. The RCP/β-TCP group showed significantly increased bone formation compared with control ($P<0.01$) and

RCP ($P<0.05$) groups. In addition, bone formation in the RCP group at 4 weeks was significantly greater than that in the control group ($P<0.05$) (Fig. 8).

4 Discussion

SEM, EDX, and cell culture assessments revealed that β-TCP fine particles dose-dependently adhered to the surface of RCP and possess excellent biocompatibility. In particular, β-TCP application promoted WST-8 activity, that is, osteoblastic cell proliferation, of RCP (Fig. 3A). Thus, it was suggested that application of β-TCP fine particles promotes positive effects on bone formation. It was reported that biomaterial surface properties including surface roughness, charge, and hydrophilicity likely affect cell adhesion and proliferation (Webb, Hlady, & Tresco, 1998; Feller et al., 2015). Accordingly, we speculated that surface modification of RCP using β-TCP fine particles increased the total surface area to adsorb protein, such as signaling molecules, to promote these cell behaviors (Ogawa et al., 2016). Some reports using bovine collagen scaffold showed a similar trend; scaffold surfaces modified with a nano-scale substance exhibited enhanced osteoblastic cell proliferation (Ibara et al., 2013; Ogawa et al., 2016; Murakami et al., 2017; Nathanael et al., 2017). Thus, surface-modified RCP likely upregulates bone formation by enhancing osteoblastic cell proliferative ability. By contrast, Murakami et al. reported that application of large amounts of β-TCP nanoparticles to the scaffold frequently cause severe inflammatory responses at the early wound healing stage (Murakami et al., 2017). Hence, the application dose of nano-substances must be investigated in detail. In this examination, application of 1% β-TCP fine particles to RCP showed low cytotoxic LDH activity, suggesting the particles would not cause adverse effects in the body.

RCP/β-TCP promoted the expression of osteogenic markers, such as Runx2, ALP, and BSP, in RT-PCR assessments (Fig. 4). Runx2 protein stimulates the differentiation of multipotent mesenchymal cells into immature osteoblasts (An et al., 2016). In addition, ALP and BSP, related to the mineralization process, are osteogenic markers used to detect the mature osteoblast (An et al., 2016). Therefore, RCP/β-TCP likely possess the potential of bone formation via osteoblastic cell differentiation. Furthermore, RCP alone stimulated the expression of these osseous markers. Because we could not detect significant differences in mRNA expression between RCP and RCP/β-TCP, osteoblastic differentiation might be induced by RCP, not applied β-TCP fine particles. Collagen type I-based recombinant peptide includes many RGD motifs to stimulate cell adhesion via integrin binding (Ruoslahti, 1996). It is well known that integrin-extracellular matrix adhesion-mediated signaling pathways are essential for osteoblastic differentiation (Schneider, Zaharias, & Stanford, 2001). Jikko et al. reported that integrin receptors of collagen regulate responses against bone morphogenetic protein-2 to consequently regulate ALP mRNA (Jikko, Harris, Chen, Mendrick, & Damsky, 1999). Schwab et al. revealed that osteogenic differentiation of mesenchymal stem cells is upregulated by RGD-containing extracellular matrix (Schwab et al., 2013). Chen et al. reported that osteoconductive bioceramics can adhere to serum proteins containing RGD motifs, subsequently increasing cell adhesion and inducing integrin expression (Chen et al., 2016). RGD-rich RCP may play a key role in bone healing and augmentation. Indeed, RCP and RCP/β-TCP stimulated mRNA expression of integrin β1 in this study (Fig. 4). Hence, we considered that RCP-applied biomaterials have bone conductive effects that may be beneficial for bone tissue engineering strategies.

Micro-CT evaluation showed that implantation of RCP and RCP/β-TCP in rat

bone defects yielded significant bone formation at 4 weeks postsurgery compared with control (no application). Furthermore, histological assessments revealed that RCP/β-TCP increased the thickness of newly formed bone compared with RCP. Terranova et al. showed that β-TCP fine particles coupled with polymer fibers induced a stimulatory effect on osteoblasts to promote bone formation of mouse (Terranova et al., 2017). In general, it is considered that β-TCP is phagocytized by macrophages and osteoclasts and provides Ca/P ions to regenerative regions (Detsch et al., 2010; Arbez, & Libouban, 2017; Arbez, Manero, Mabilleau, Libouban, & Chappard, 2019). In immunostaining assessments, CD68-positive macrophages frequently appeared on the surface of RCP/β-TCP, but not on the surface of newly formed bone (Fig. 6), suggesting that RCP/β-TCP are degraded by macrophages. Reportedly, Ca ions stimulate the expression of osseous markers in osteoblastic cells and then adjust the *in vivo* environment for bone generation (Lee et al., 2018). In addition, Ca ion concentration regulates osteoblast proliferation and differentiation (Maeno et al., 2005). In this study, residual β-TCP was rarely found in histological specimens at 2 weeks postsurgery, thereby suggesting that β-TCP particles appeared to be well-degraded and likely related to processes proceeding bone formation. From *in vitro* evaluations, it was considered that RCP/β-TCP synergistically provide two biological effects: cell proliferation by β-TCP fine particles and cell differentiation by RGD-rich motif, to consequently facilitate early bone formation. Osteocalcin-stained samples at 2 weeks postsurgery exhibited the osteoblast-inducing ability of RCP/β-TCP (Fig. 6). These properties of RCP/β-TCP as the bone filling scaffold material will yield great advantages for regenerative tissue quality and quantity in bone tissue engineering therapy. However, in this study, collagen xenograft (no modifying RGD motif recombinantly) applied with

β-TCP fine particles was not evaluated. Additional studies are needed to analyze whether the bone forming ability of RCP/β-TCP is superior to conventional collagen graft/β-TCP.

Conclusion

We herein assessed the cytocompatibility and bone forming ability of RCP and RCP/β-TCP. The results showed that RCP/β-TCP promote osteoblast proliferation and exhibit low cytotoxicity. Real-time RT-PCR examination showed that RCP and RCP/β-TCP stimulate mRNA expression of integrin β1 and osteogenic markers, regardless of the application of β-TCP fine particles. In histometric assessment in rat, the RCP/β-TCP group showed significant bone formation compared with RCP and control (no application) groups. Hence, RCP/β-TCP exhibit osteogenic capability and would be beneficial for bone tissue engineering therapy.

Acknowledgments

The authors thank FUJIFILM Corp. and Taihei Chemical Industrial Co., Ltd., for providing primary reagents. EDX analysis was carried out with FE-SEM at the Joint-use Facilities: Laboratory of Nano-Micro Material Analysis at Hokkaido University. This work was supported by JPSP KAKENHI (grant nos. JP16K11822 and JP18K17038) and AMED translational research program (grant nos. A105 and A154).

Conflict of interest

The authors report that they have no conflict of interest related to this study.

References

1) An J, Yang H, Zhang Q, Liu C, Zhao J, Zhang L, Chen B. 2016. Natural products for treatment of osteoporosis: The effects and mechanisms on promoting osteoblast-mediated bone formation. *Life Sci* 147:46-58.
2) Arbez B, Libouban H. 2017. Behavior of macrophage and osteoblast cell lines in contact with the β-TCP biomaterial (beta-tricalcium phosphate). *Morphologie*. 101:154-163.
3) Arbez B, Manero F, Mabilleau G, Libouban H, Chappard D. 2019. Human macrophages and osteoclasts resorb β-tricalcium phosphate in vitro but not mouse macrophages. *Micron*. 125:102730.
4) Bose S, Roy M, Bandyopadhyay A. 2012. Recent advances in bone tissue engineering scaffolds. *Trends Biotechnol* 30:546-554.
5) Carrel JP, Wiskott A, Moussa M, Rieder P, Scherrer S, Durual S. 2016. A 3D printed TCP/HA structure as a new osteoconductive scaffold for vertical bone augmentation. *Clin Oral Implants Res* 27:55-62.
6) Chen X, Wang J, Chen Y, Cai H, Yang X, Zhu X, Fan Y, Zhang X. 2016. Roles of calcium phosphate-mediated integrin expression and MAPK signaling pathways in the osteoblastic differentiation of mesenchymal stem cells. *J Mater Chem B* 4:2280-2289.
7) Cuervo-Lozano CE, Soto-Domínguez A, Saucedo-Cárdenas O, Montes-de-Oca-Luna R, Alonso-Romero S, Del Consuelo Mancías-Guerra M, Álvarez-Lozano E. 2018. Osteogenesis induced by a three-dimensional bioimplant composed of demineralised bone matrix, collagen, hydroxyapatite, and bone marrow-derived cells in massive bone defects: An experimental study. *Tissue Cell*

50:69-78.

8) Detsch R, Hagmeyer D, Neumann M, Schaefer S, Vortkamp A, Wuelling M, Ziegler G, Epple M. 2010. The resorption of nanocrystalline calcium phosphates by osteoclast-like cells. *Acta Biomater*. 6:3223-3233.

9) Diederichs S, Böhm S, Peterbauer A, Kasper C, Scheper T, van Griensven M. 2010. Application of different strain regimes in two-dimensional and three-dimensional adipose tissue-derived stem cell cultures induces osteogenesis: implications for bone tissue engineering. *J Biomed Mater Res A* 94:927-36.

10) Fawzy El-Sayed KM, Mekhemar MK, Beck-Broichsitter BE, Bähr T, Hegab M, Receveur J, Heneweer C, Becker ST, Wiltfang J, Dörfer CE. 2015. Periodontal regeneration employing gingival margin-derived stem/progenitor cells in conjunction with IL-1ra-hydrogel synthetic extracellular matrix. *J Clin Periodontol* 42:448-457.

11) Feller L, Jadwat Y, Khammissa RA, Meyerov R, Schechter I, Lemmer J. 2015. Cellular responses evoked by different surface characteristics of intraosseous titanium implants. *Biomed Res Int* 2015:171945.

12) Hamlet SM, Vaquette C, Shah A, Hutmacher DW, Ivanovski S. 2017. 3-Dimensional functionalized polycaprolactone-hyaluronic acid hydrogel constructs for bone tissue engineering. *J Clin Periodontol* 44:428-437.

13) Ibara A, Miyaji H, Fugetsu B, Nishida E, Takita H, Tanaka S, Sugaya T, Kawanami M. 2013. Osteoconductivity and biodegradability of collagen scaffold coated with nano-β-TCP and fibroblast growth factor 2. *J Nanomater* 2013:639502.

14) Jikko A, Harris SE, Chen D, Mendrick DL, Damsky CH. 1999. Collagen integrin receptors regulate early osteoblast differentiation induced by BMP-2. *J Bone Miner*

Res 14:1075-1083.

15) Kakar A, Rao BHS, Hegde S, Deshpande N, Lindner A, Nagursky H, Patney A, Mahajan H. 2017. Ridge preservation using an in situ hardening biphasic calcium phosphate (β-TCP/HA) bone graft substitute-a clinical, radiological, and histological study. *Int J Implant Dent* 3:25.

16) Kim S, Lee S, Kim K. 2018. Bone tissue engineering strategies in co-delivery of bone morphogenetic protein-2 and biochemical signaling factors. *Adv Exp Med Biol* 1078:233-244.

17) Kuttappan S, Mathew D, Nair MB. 2016. Biomimetic composite scaffolds containing bioceramics and collagen/gelatin for bone tissue engineering - A mini review. *Int J Biol Macromol* 93:1390-1401.

18) Mashiko T, Takada H, Wu SH, Kanayama K, Feng J, Tashiro K, Asahi R, Sunaga A, Hoshi K, Kurisaki A, Takato T, Yoshimura K. 2018. Therapeutic effects of a recombinant human collagen peptide bioscaffold with human adipose-derived stem cells on impaired wound healing after radiotherapy. *J Tissue Eng Regen Med* 12:1186-1194.

19) Lee MN, Hwang HS, Oh SH, Roshanzadeh A, Kim JW, Song JH, Kim ES, Koh JT. 2018. Elevated extracellular calcium ions promote proliferation and migration of mesenchymal stem cells via increasing osteopontin expression. *Exp Mol Med* 50:142.

20) Maeno S, Niki Y, Matsumoto H, Morioka H, Yatabe T, Funayama A, Toyama Y, Taguchi T, Tanaka J. 2005. The effect of calcium ion concentration on osteoblast viability, proliferation and differentiation in monolayer and 3D culture. *Biomaterials* 26:4847-4855.

21) Miyamoto M, Nakamura K, Shichinohe H, Yamauchi T, Ito M, Saito H, Kawabori M, Osanai T, Sasaki T, Houkin K, Kuroda S. 2018. Human recombinant peptide sponge enables novel, less invasive cell therapy for ischemic stroke. *Stem Cells Int* 2018:4829534.

22) Murakami S, Miyaji H, Nishida E, Kawamoto K, Miyata S, Takita H, Akasaka T, Fugetsu B, Iwanaga T, Hongo H, Amizuka N, Sugaya T, Kawanami M. 2017. Dose effects of beta-tricalcium phosphate nanoparticles on biocompatibility and bone conductive ability of three-dimensional collagen scaffolds. *Dent Mater J* 36:573-583.

23) Nathanael AJ, Oyane A, Nakamura M, Sakamaki I, Nishida E, Kanemoto Y, Miyaji H. 2017. In vitro and in vivo analysis of mineralized collagen-based sponges prepared by a plasma- and precursor-assisted biomimetic process. *ACS Appl Mater Interfaces* 9:22185-22194.

24) Ogawa K, Miyaji H, Kato A, Kosen Y, Momose T, Yoshida T, Nishida E, Miyata S, Murakami S, Takita H, Fugetsu B, Sugaya T, Kawanami M. 2016. Periodontal tissue engineering by nano beta-tricalcium phosphate scaffold and fibroblast growth factor-2 in one-wall infrabony defects of dogs. *J Periodont Res* 51:758-767.

25) Oh KJ, Ko YB, Jaiswal S, Whang IC. 2016. Comparison of osteoconductivity and absorbability of beta-tricalcium phosphate and hydroxyapatite in clinical scenario of opening wedge high tibial osteotomy. *J Mater Sci Mater Med* 27:179.

26) OKeefe RJ, Mao J. 2011. Bone tissue engineering and regeneration: from discovery to the clinic--an overview. *Tissue Eng Part B Rev* 17:389-392.

27) Parvizi M, Plantinga JA, van Speuwel-Goossens CA, van Dongen EM, Kluijtmans SG, Harmsen MC. 2016. Development of recombinant collagen-peptide-based

vehicles for delivery of adipose-derived stromal cells. *J Biomed Mater Res A* 104:503-516.

28) Pawelec KM, Confalonieri D, Ehlicke F, van Boxtel HA, Walles H, Kluijtmans SGJM. 2017. Osteogenesis and mineralization of mesenchymal stem cells in collagen type I-based recombinant peptide scaffolds. *J Biomed Mater Res A* 105:1856-1866.

29) Perez JR, Kouroupis D, Li DJ, Best TM, Kaplan L, Correa D. 2018. Tissue engineering and cell-based therapies for fractures and bone defects. *Front Bioeng Biotechnol* 6:105.

30) Peticone C, De Silva Thompson D, Owens GJ, Kim HW, Micheletti M, Knowles JC, Wall I. 2017. Towards modular bone tissue engineering using Ti-Co-doped phosphate glass microspheres: cytocompatibility and dynamic culture studies. *J Biomater Appl* 32:295-310.

31) Pfaffl MW. 2001. A new mathematical model for relative quantification in real-time RT-PCR. *Nucleic Acids Res* 29:e45.

32) Ruoslahti E. 1996. RGD and other recognition sequences for integrins. *Annu Rev Cell Dev Biol* 12:697-715.

33) Schmittgen TD, Zakrajsek BA. 2000. Effect of experimental treatment on housekeeping gene expression: validation by real-time, quantitative RT-PCR. *J Biochem Biophys Methods* 46:69–81.

34) Schneider GB, Zaharias R, Stanford C. 2001. Osteoblast integrin adhesion and signaling regulate mineralization. *J Dent Res* 80:1540-1544.

35) Schwab EH, Halbig M, Glenske K, Wagner AS, Wenisch S, Cavalcanti-Adam EA. 2013. Distinct effects of RGD-glycoproteins on integrin-mediated adhesion and

osteogenic differentiation of human mesenchymal stem cells. *Int J Med Sci* 10:1846-1859.

36) Sheikh FA, Ju HW, Moon BM, Lee OJ, Kim JH, Park HJ, Kim DW, Kim DK, Jang JE, Khang G, Park CH. 2016. Hybrid scaffolds based on PLGA and silk for bone tissue engineering. *J Tissue Eng Regen Med* 10:209-221.

37) Terranova L, Dragusin DM, Mallet R, Vasile E, Stancu IC, Behets C, Chappard D. 2017. Repair of calvarial bone defects in mice using electrospun polystyrene scaffolds combined with β-TCP or gold nanoparticles. Micron. 93:29-37.

38) Thomason LC, Sawitzke JA, Li X, Costantino N, Court DL. 2014. Recombineering: genetic engineering in bacteria using homologous recombination. *Curr Protoc Mol Biol* 106:1.16.1-39.

39) Webb K, Hlady V, Tresco PA. 1998. Relative importance of surface wettability and charged functional groups on NIH 3T3 fibroblast attachment, spreading, and cytoskeletal organization. *J Biomed Mater Res* 41:422-430.

40) Xing ZC, Han SJ, Shin YS, Koo TH, Moon S, Jeong Y, Kang IK. 2013. Enhanced osteoblast responses to poly(methyl methacrylate)/hydroxyapatite electrospun nanocomposites for bone tissue engineering. *J Biomater Sci Polym Ed*. 24:61-76.

41) Yin J, Qiu S, Shi B, Xu X, Zhao Y, Gao J, Zhao S, Min S. 2018. Controlled release of FGF-2 and BMP-2 in tissue engineered periosteum promotes bone repair in rats. *Biomed Mater* 13:025001.

42) Zhu Q, Lu C, Jiang X, Yao Q, Jiang X, Huang Z, Jiang Y, Peng L, Fu H, Zhao Y. 2020. Using recombinant human collagen with basic fibroblast growth factor to provide a simulated extracellular matrix microenvironment for the revascularization and attachment of islets to the transplantation region. *Front Pharmacol* 10:1536.

43) Zijderveld SA, Zerbo IR, van den Bergh JP, Schulten EA, ten Bruggenkate CM. 2005. Maxillary sinus floor augmentation using a beta-tricalcium phosphate (Cerasorb) alone compared to autogenous bone grafts. *Int J Oral Maxillofac Implants* 20:432-440.

Figures

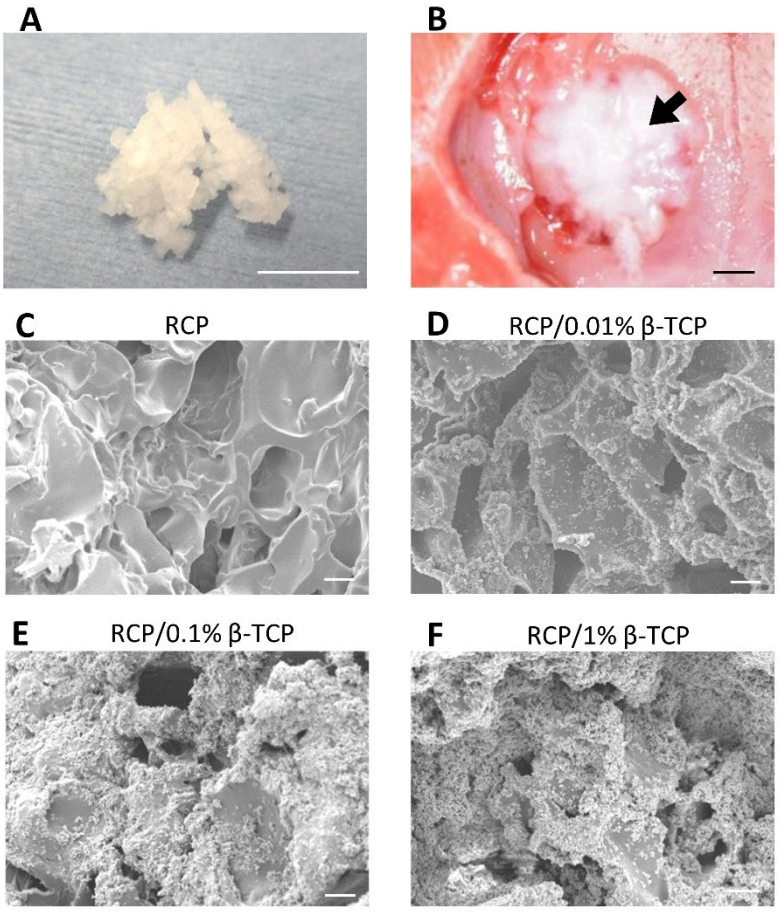

Figure 1. Digital photographs and SEM images

(A) Digital photograph of RCP/1% β-TCP. (B) Implantation of RCP/1% β-TCP (arrow) into the rat cranial bone defect. (C–F) SEM images of RCP and RCP/0.01, 0.1, and 1% β-TCP. Scale bars represent 10 mm (A), 1 mm (B), and 10 μm (C–F).

Abbreviations: RCP, granules containing recombinant human collagen peptide; β-TCP, β-tricalcium phosphate; SEM, scanning electron microscope.

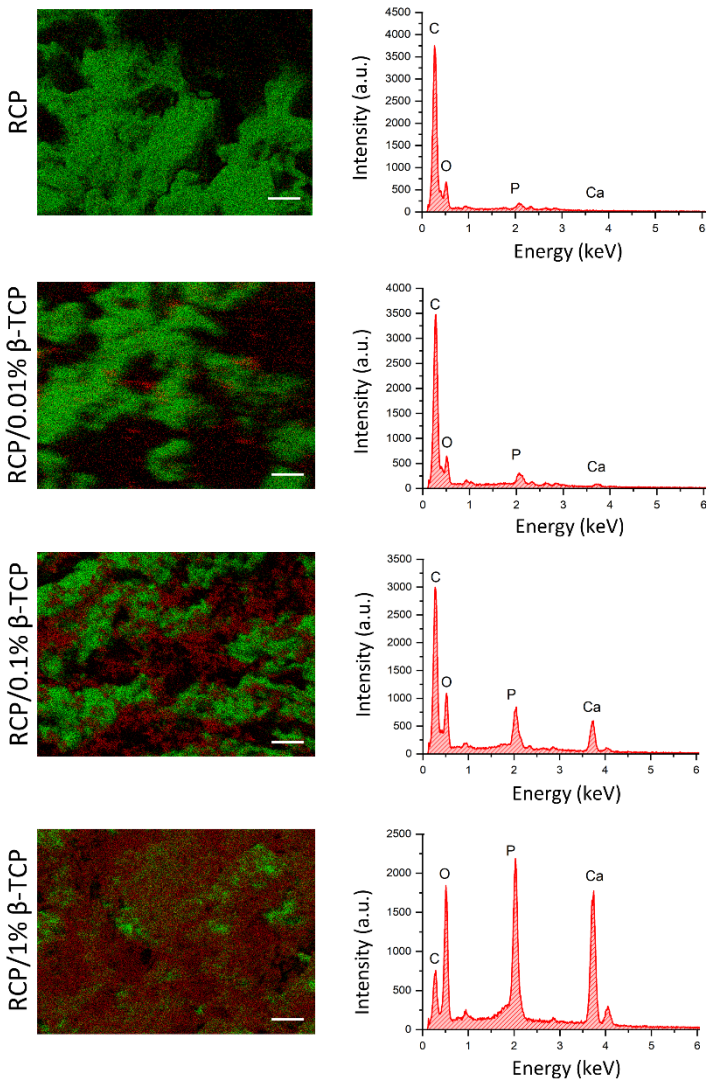

Figure 2. EDX analysis

Ca and C were stained in red and green, respectively. Scale bars represent 10 μm.

Abbreviations: EDX, energy dispersive X-ray spectrometry; RCP, granules containing recombinant human collagen peptide; β-TCP, β-tricalcium phosphate.

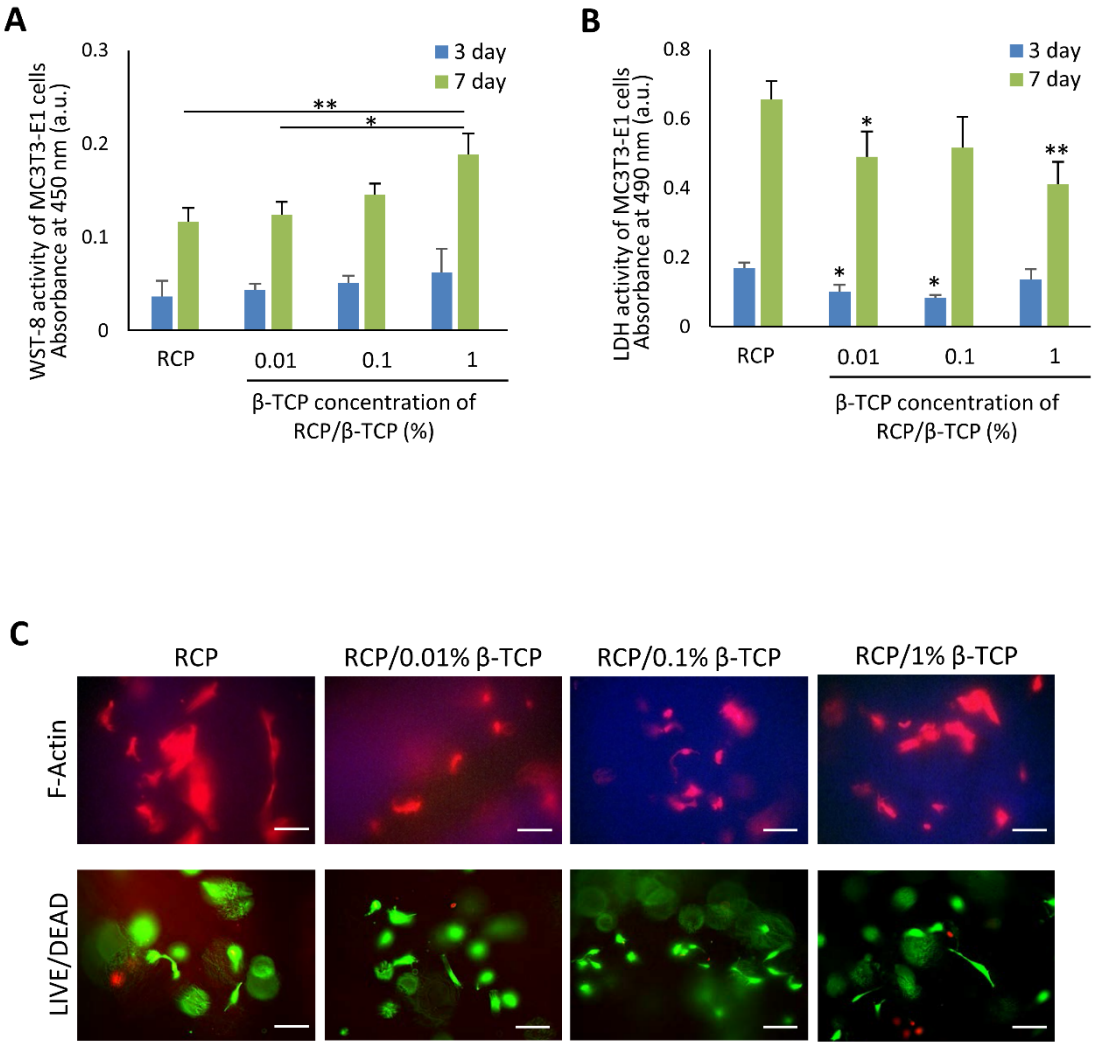

Figure 3. Assessments of cytocompatibility

(A) WST-8 activity of MC3T3-E1 cells (N=4, mean ± SD). *P<0.05, **P<0.01. (B) LDH activity of MC3T3-E1 cells (N=4, mean ± SD). *P<0.05, **P<0.01 vs. RCP. (C) Microscopic images of F-actin (stained in red) and LIVE/DEAD BacLight staining (live in green, dead in red) of MC3T3-E1 cells after 24-h incubation. All samples consistently exhibited live cells. Scale bar represents 100 μm.

Abbreviations: WST-8, water-soluble tetrazolium salts-8; RCP, granules containing recombinant human collagen peptide; β-TCP, β-tricalcium phosphate; LDH, lactate dehydrogenase.

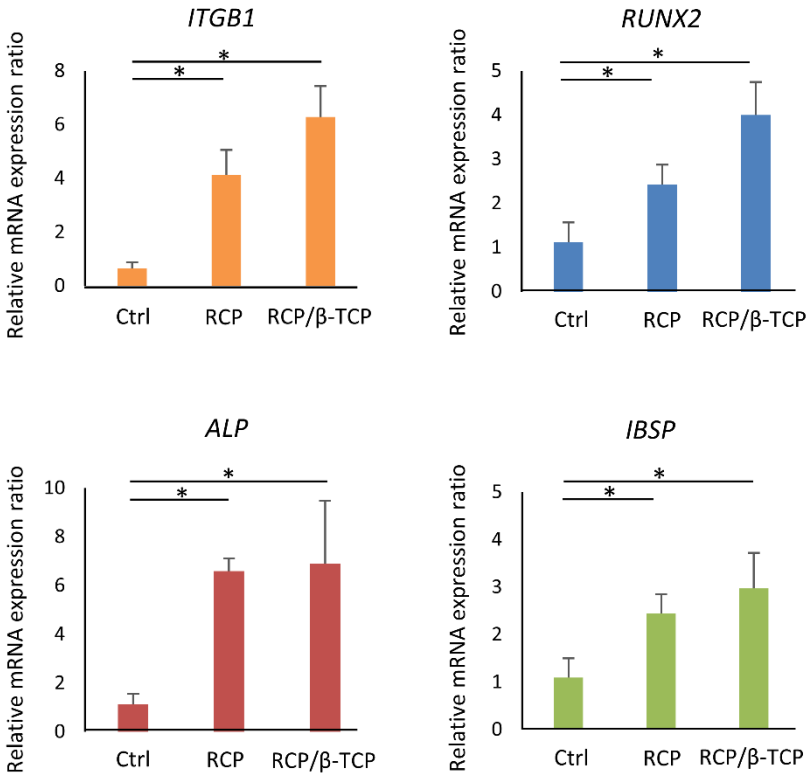

Figure 4. Assessments of RT-PCR

Measurements of the expression of mouse *ITGB1*, *RUNX2*, *ALP*, and *IBSP* by RT-PCR (N=4, mean ± SD). *P<0.05.

Abbreviations: ALP, alkaline phosphatase; IBSP, bone sialoprotein; ITGB1, integrin β1; RCP, granules containing recombinant human collagen peptide; RT-PCR, reverse transcription polymerase chain reaction; RUNX2, runt-related transcription factor 2; β-TCP, β-tricalcium phosphate.

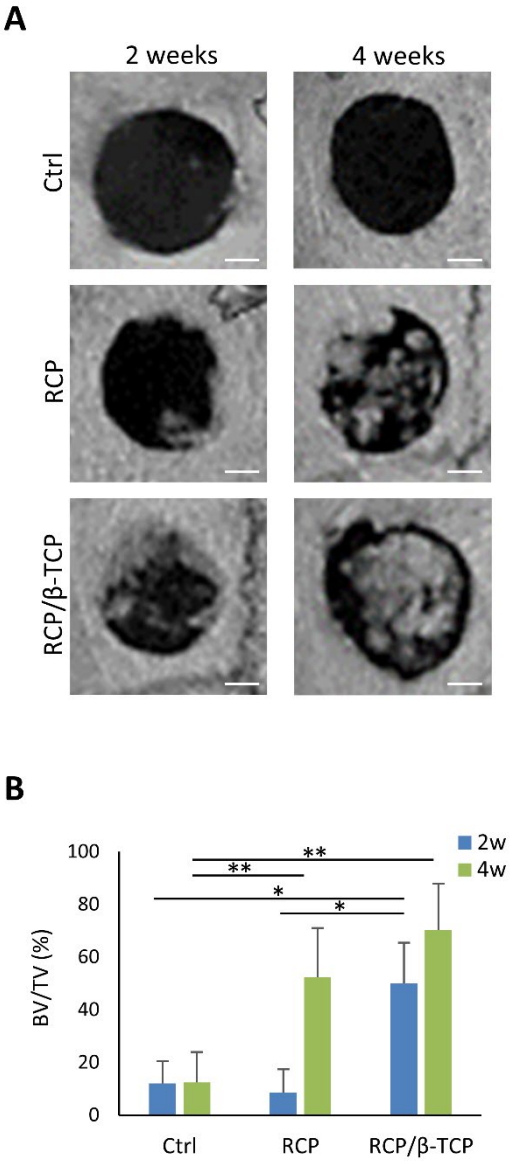

Figure 5. Micro-CT analysis

(A) Micro-CT images of Ctrl, RCP, and RCP/β-TCP groups at 2 and 4 weeks postsurgery. Scale bar represents 1 mm. (B) Percent bone volume (BV/TV) at 2 and 4 weeks postsurgery (N=6, mean ± SD). *P<0.05, **P<0.01.

Abbreviations: Micro-CT, micro computed tomography; Ctrl, control (no application of RCP or RCP/β-TCP); RCP, granules containing recombinant human collagen peptide; β-TCP, β-tricalcium phosphate.

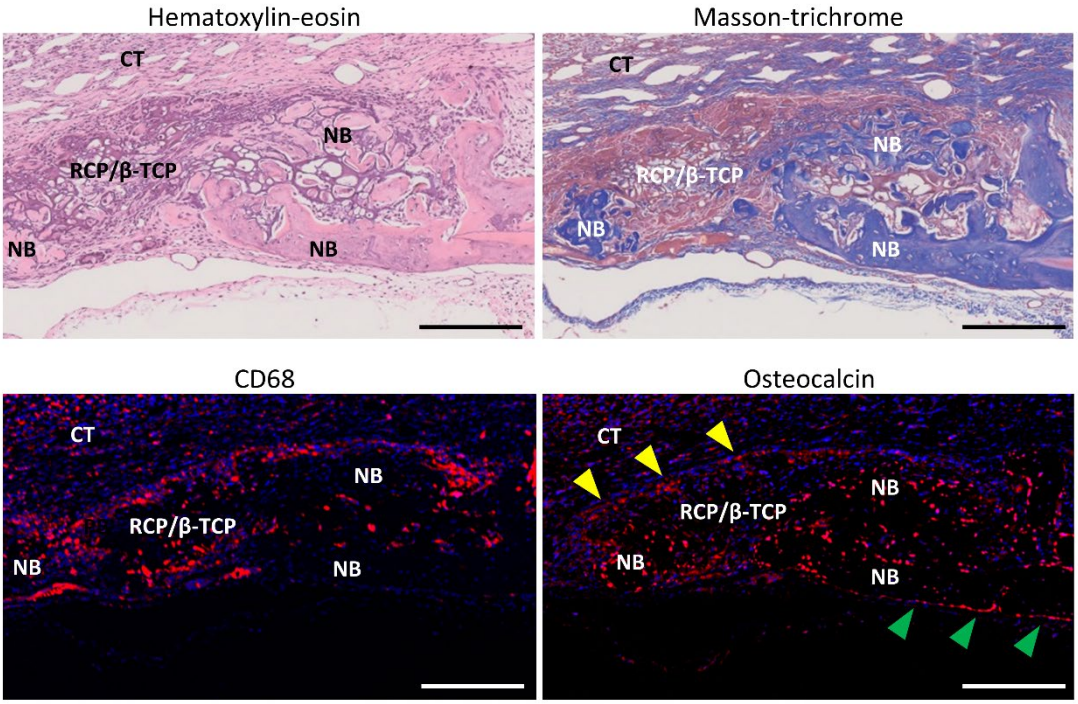

Figure 6. Histological findings of RCP/β-TCP at 2 weeks after implantation in rat

CD68-positive macrophages and osteocalcin-positive osteoblastic cells are stained in red. Osteoblastic cells were observed on newly formed bone (green arrowheads) and RCP/β-TCP residue (yellow arrowheads). Scale bar represents 200 μm.

Abbreviations: CT, connective tissue; NB, new bone; RCP, granules containing recombinant human collagen peptide; β-TCP, β-tricalcium phosphate.

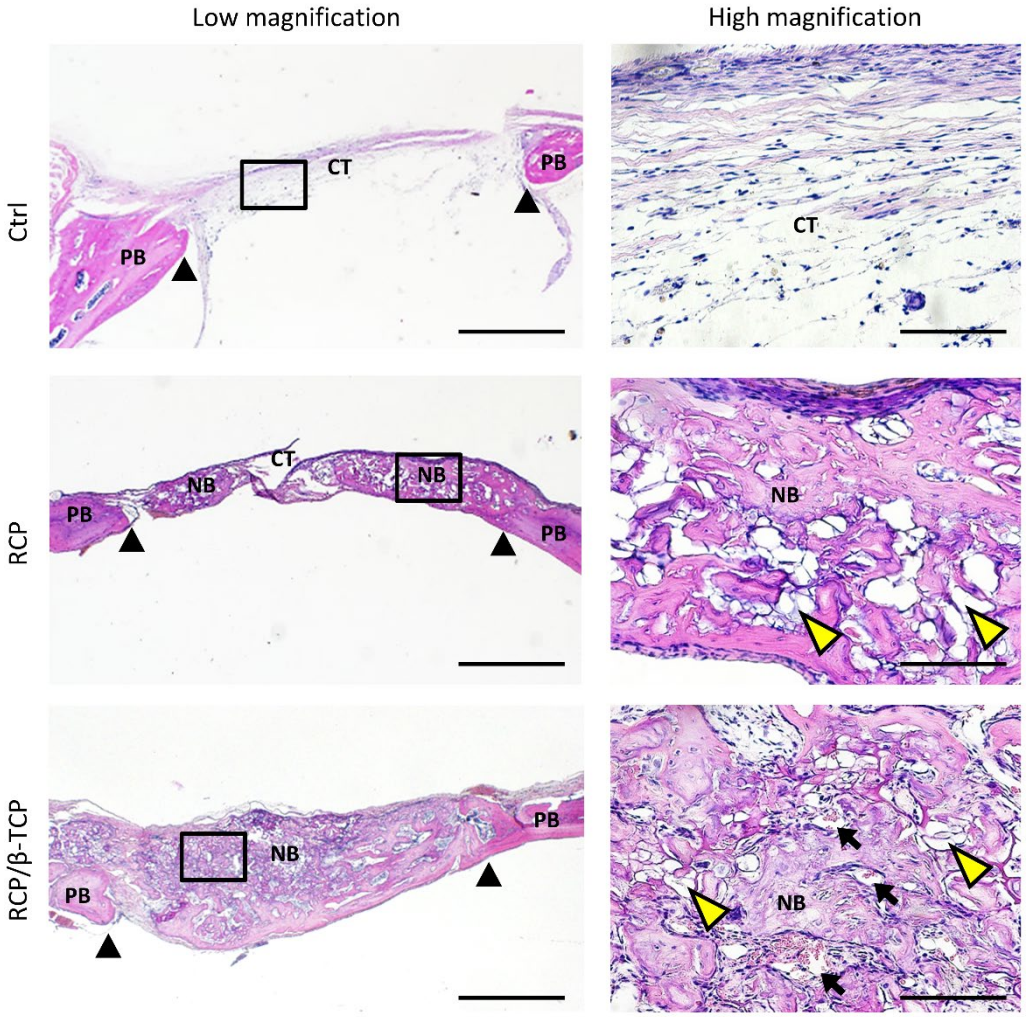

Figure 7. Histological findings at 4 weeks after implantation in rat

High magnification images related to framed areas in low magnification images. Scale bar represents 1 mm (low magnification) and 100 μm (high magnification). Black arrowheads in low magnification images indicate the border of the bone defect. Yellow arrowheads in high magnification images indicate residual RCP or RCP/β-TCP. Black arrows indicate blood vessels. Staining: hematoxylin and eosin.

Abbreviations: CT, connective tissue; NB, new bone; PB, preexisting bone; RCP, granules containing recombinant human collagen peptide; β-TCP, β-tricalcium phosphate.

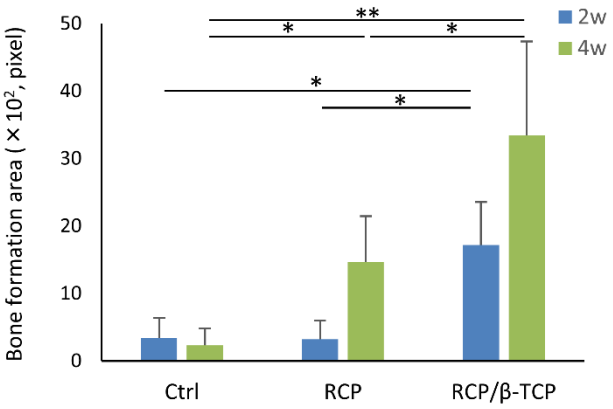

Figure 8. Histomorphometric measurements of bone formation

Bone formation area at 2 and 4 weeks after implantation in rat (N=6, mean ± SD). *P<0.05, **P<0.01.

Abbreviations: Ctrl, control; RCP, granules containing recombinant human collagen peptide; β-TCP, β-tricalcium phosphate.